Atmos. Meas. Tech. Discuss., 6, 2979–3011, 2013
www.atmos-meas-tech-discuss.net/6/2979/2013/
doi:10.5194/amtd-6-2979-2013

Atmospheric Measurement Techniques Discussions

Ground-based stratospheric O_3 and HNO_3 measurements at Thule, Greenland: an intercomparison with Aura MLS observations

I. Fiorucci[1], G. Muscari[1], L. Froidevaux[2], and M. L. Santee[2]

[1]Istituto Nazionale di Geofisica e Vulcanologia, Roma, Italy
[2]Jet Propulsion Laboratory, California Institute of Technology, Pasadena, California, USA

Received: 24 December 2012 – Accepted: 4 March 2013 – Published: 25 March 2013

Correspondence to: I. Fiorucci (irene.fiorucci@ingv.it)

Published by Copernicus Publications on behalf of the European Geosciences Union.

Abstract

In response to the need for improving our understanding of the evolution and the interannual variability of the winter Arctic stratosphere, in January 2009 a ground-based millimeter-wave spectrometer (GBMS) was installed at the Network for the Detection of Atmospheric Composition Change (NDACC) site in Thule (76.5° N, 68.8° W), Greenland. In this work, stratospheric GBMS O_3 and HNO_3 vertical profiles obtained from Thule during winters 2010 (HNO_3 only), 2011 and 2012 are characterized and intercompared with co-located Aura MLS measurements. Using a recently developed algorithm based on Optimal Estimation, we find that the GBMS O_3 retrievals show good sensitivity (> 80 %) to atmospheric variations between ∼ 17 and ∼ 50 km, where their 1 σ uncertainty is estimated to be the larger of ∼ 11% or 0.2 ppmv. Similarly, HNO_3 profiles can be considered for scientific use between ∼ 17 and ∼ 45 km altitude, with a 1 σ uncertainty that amounts to the larger of 15 % or 0.2 ppbv. Comparisons with Aura MLS version 3.3 observations show that, on average, GBMS O_3 mixing ratios are biased low with respect to MLS throughout the stratosphere, with differences ranging between ∼ 0.3 ppmv (8 %) and 0.9 ppmv (18 %) in the 17–50 km vertical range. GBMS HNO_3 values display instead a high bias with respect to MLS up to 26 km, reaching a maximum of ∼ 1 ppbv (10 %) near the mixing ratio profile peak. O_3 and HNO_3 values from the two data sets prove to be well correlated at all altitudes, although their correlations worsen at the lower end of the altitude ranges considered. Column contents of GBMS and MLS O_3 (from 20 km upwards) and HNO_3 (from 17 km upwards) correlate very well and indicate that GBMS measurements can provide valuable estimates of column interannual and seasonal variations for these compounds.

AMTD
6, 2979–3011, 2013

1 Introduction

Driven by increasing concerns about anthropogenic ozone reduction, microwave spectroscopy started to be employed in the early 1980s to study various stratospheric constituents involved in the ozone depletion processes (e.g., Parrish et al., 1988, 1992; de Zafra et al., 1987; Connor et al., 1987; Waters et al., 1993). Together with chlorine compounds, HNO_3 plays a key role in these processes. It is a primary reservoir for reactive nitrogen in the stratosphere and one of the main components of the Polar Stratospheric Clouds (PSCs) which provide surfaces for heterogeneous chemical conversion of chlorine from its reservoir species (HCl, $ClONO_2$) into highly reactive ozone-destroying forms (Cl, ClO) (Solomon, 1990).

Starting in 1993 observations of stratospheric O_3 and HNO_3 have been carried out by means of a Ground-Based Millimeter-wave Spectrometer (GBMS) at different sites in both hemispheres, at polar and mid-latitudes (e.g., de Zafra et al., 1997; Muscari et al., 2007; Santee et al., 2007). GBMS data have contributed to shed light on processes related to the global ozone decline and to the dramatic ozone loss occurring over the Antarctic continent every spring. In particular, in 1993 the GBMS provided the first quasi-continuous year-long data record of HNO_3 and O_3 vertical profiles in the heart of the south polar vortex showing the direct link between the appearance of PSCs and the rapid removal of HNO_3 from the lower stratosphere (de Zafra et al., 1997). Since then a continuous monitoring of the stratospheric composition changes in response to the anthropogenic forcing (including ozone depleting substances release) has been carried out by the Network for the Detection of Stratospheric Change (NDSC), now Network for the Detection of Atmospheric Composition Change (NDACC). The microwave spectroscopy has been used to measure different stratospheric trace gases since the constitution of the NDSC/NDACC and a number of spectrometers are now operational in several of its more than 70 remote-sensing stations covering all latitudinal bands (Boyd et al., 2007; Connor et al., 2007; Hafele et al., 2009; Nedoluha et al., 2011).

AMTD
6, 2979–3011, 2013

Although initially polar ozone research was mainly focused on the Antarctic (where the winter/spring ozone loss between 14 and 20 km is regularly close to 100 %), in the past few years the attention has shifted towards similar but less understood mechanisms that are at work in the Arctic. The main processes leading to ozone reduction are the same over the two poles but pronounced differences in stratospheric dynamics between the two hemispheres lead to larger interannual variability in the stratospheric temperatures and in the vortex stability over the Arctic with respect to what occurs over the Antarctic (e.g., Harris et al., 2010). We lack a complete understanding of mechanisms driving this variability and of potential effects that increasing greenhouse gases may have on these processes (Manney et al., 2011). Present day Chemistry Climate Models (CCMs) underestimate the observed frequency of cold Arctic winters (WMO, 2010) and do not capture the long-term trend of the coldest winters becoming colder (Rex et al., 2006). A cooling of the polar lower stratosphere is expected to increase the occurrence and the duration of PSCs, especially in the Arctic, where observed temperatures are frequently close to the PSC formation threshold. Therefore, this general warm bias in CCMs results in the Arctic may lead to a significant underestimation of the chemical ozone loss in the Northern Hemisphere, especially while anthropogenic halogen levels remain elevated (WMO, 2010). Improving our knowledge and our predictive capabilities for the evolution of the Arctic stratosphere is one of the main atmospheric challenges of the next decades, and comprehensive long-term stratospheric data records, such as those provided by the instruments deployed in the NDACC Arctic stations (Palm et al., 2010; Hoffman et al., 2011), are a prerequisite to reach this goal.

In order to address these needs, in January 2009 the GMBS was installed at the NDACC Arctic station located at Thule (76.5° N, 68.8° W), Greenland, with the purpose of establishing a long-term observation site. Since then, four winter campaigns have been carried out during the period January–March 2009–2012 (Di Biagio et al., 2010; Muscari et al., 2012), and regular winter campaigns are planned for the future.

In the past, GBMS O_3 and HNO_3 spectra were deconvolved using a Chahine-Twomey (C-T) (Twomey et al., 1977) and an iterative constrained Matrix Inversion (MI)

AMTD
6, 2979–3011, 2013

technique (Twomey, 1977), respectively. More recently, the GBMS retrieval algorithm has been updated to an Optimal Estimation method in order to conform to the standard of the NDACC microwave group, and to easily provide retrievals with a set of Averaging Kernels that grants more straightforward comparisons with other data sets (Fiorucci et al., 2011). Comparing ground-based measurements with satellite observations is particularly important because, if well-validated, the ground-based data may be used to fill gaps in temporal coverage of satellite data sets. Such a gap is likely to occur in this decade, when most of the satellite missions that in the past decade have provided an accurate and global picture of the stratosphere are not expected to be replaced by follow-up missions. In this study we present GBMS stratospheric O_3 and HNO_3 measurements obtained during the last two (for O_3) or three (for HNO_3) winters at Thule, illustrating briefly the main characteristic of the observing technique and the adaptation of the Optimal Estimation method to GBMS spectra. Furthermore, the accuracy of the presented data is assessed through comparisons with correlative satellite data sets from the Aura Microwave Limb Sounder (MLS) experiment.

2 GBMS observing technique

The GBMS is a heterodyne spectrometer that measures O_3 and other stratospheric trace gases (such as HNO_3, N_2O and CO) relevant to ozone chemistry and transport in the polar regions by observing rotational transition lines emitted from these constituents between 230 and 280 GHz. Its initial prototype was designed and built at the State University of New York at Stony Brook (de Zafra, 1995) at the end of the 1980s, when increasing interest in polar ozone depletion processes developed in the atmospheric scientific community. In its present form it consists of a high sensitivity cryogenically cooled heterodyne receiver, followed by two Acousto-Optical Spectrometers: the so-called "wide-band" spectrometer with a bandpass of 600 MHz and a resolution of 1.176 MHz, and the "narrow-band" spectrometer with a spectral window of 50 MHz and a resolution of ~65 kHz. The strong dependence of the line broadening

AMTD
6, 2979–3011, 2013

on the atmospheric pressure profile allows for the retrieval of mixing ratio vertical profiles of the observed species, using deconvolution algorithms. The overall spectral band pass and resolution of the spectrometer used are therefore key elements to determine the altitude range over which trace gases concentration can be measured. In particular, vertical profiles of the observed trace gases can be retrieved between ∼15 and ∼50 km and between ∼35 and ∼80 km using the GBMS wide-band and narrow-band spectrometers, respectively.

The GBMS observational geometry relies on the beam switching technique first described by Parrish et al. (1988) and widely employed in millimeter-wave spectroscopy. A detailed discussion of the GBMS observing technique and involved equations can be found in de Zafra (1995) and Fiorucci et al. (2008).

GBMS O_3 measurements discussed in this work are obtained by observing the pure rotational transition line at 264.925 GHz (Fig. 1a). The observed HNO_3 spectrum is more complex and characterized by a number of superimposed, relatively weak rotational lines centered at 269.240 GHz, appearing as a compact cluster in the spectrometer pass band due to pressure broadening (Fig. 2a). In this spectral window the wing of a strong O_3 line is visible and contributes background curvature to the HNO_3 spectra. GBMS spectra are initially saved in 15 min integration time bins but ultimately averaged together in 1–2 h (for O_3) or 3–6 h (for the weaker HNO_3 lines) bins to improve the signal-to-noise ratio (S/N).

Since this work is focused on stratospheric O_3 and HNO_3, only wide-band spectral data will be discussed. Upper stratospheric/mesospheric O_3 observations obtained from the GBMS narrow-band spectrometer have already been presented by Muscari et al. (2012).

3 GBMS data set

Out of the four winter campaigns carried out at Thule during the first three months (January–March) of 2009, 2010, 2011, and 2012, the O_3 and HNO_3 ground-based

AMTD
6, 2979–3011, 2013

observations presented in this work have been obtained only during the last two (for O_3) or three (for HNO_3) campaigns. During all the campaigns, measurements have been performed mostly on a daily basis, except in cases of poor weather conditions, for a total of 106 days.

Due to an instrument malfunction, during the first measurement campaign, in 2009, the observed spectra showed baseline artifacts (usually absent in the GBMS spectra) which rendered the uncertainties in the retrieval of the weak and complex HNO_3 spectra exceedingly high, and these data were therefore discarded for the comparison with MLS data. As for O_3 measurements, starting in January 2011 the O_3 line observed by the GBMS was changed from the one at 276.923 GHz to the emission at 264.925 GHz, due to better sensitivity of the GBMS in the latter frequency range. Although observations of the two transition lines yield O_3 data that are consistent overall, because of the large variability of stratospheric O_3 during each Arctic winter and from one winter to the next, we employ only the 2011 and 2012 O_3 data obtained with better sensitivity at 264.925 GHz for the intercomparison with Aura MLS. This is the emission line that the GBMS will continue to observe in future Arctic campaigns.

In order to retrieve mixing ratio vertical profiles from GBMS spectra, an Optimal Estimation (OE) algorithm is used. A detailed description of the OE algorithm is given by Rodgers (1976, 2000), while the adaptation of the general theory to GBMS measurements has been extensively presented in Fiorucci et al. (2011) and Muscari et al. (2012). Here we briefly illustrate only those aspects of the GBMS inversion technique necessary to better characterize the retrieved profiles presented in this work.

The OE method combines information coming from the a priori profile ($\boldsymbol{x}_a$) and from the measurements ($\boldsymbol{y}$), weighting their contributions with the respective inverse covariances ($\mathbf{S}_\varepsilon^{-1}$) and ($\mathbf{S}_a^{-1}$). The retrieval solution is given by:

AMTD
6, 2979–3011, 2013

$$\boldsymbol{x} = \frac{\mathbf{S}_\mathrm{a}^{-1}\boldsymbol{x}_\mathrm{a} + \mathbf{K}^T\mathbf{S}_\varepsilon^{-1}\boldsymbol{y}}{\mathbf{S}_\mathrm{a}^{-1} + \mathbf{K}^T\mathbf{S}_\varepsilon^{-1}\mathbf{K}} \quad (1)$$

where the weighting functions **K** describe the sensitivity of the spectrum to changes in the true atmospheric profile. The amount of information that is added to $\boldsymbol{x}_\mathrm{a}$ from the measurement depends on the physical (forward) model included in **K**, as well as on the error covariances $\mathbf{S}_\varepsilon$ and $\mathbf{S}_\mathrm{a}$ (in particular on the ratio $\mathbf{S}_\varepsilon$ to $\mathbf{S}_\mathrm{a}$ rather than on their absolute values). In fact, assigning a small uncertainty to the a priori profile constrains the retrieved profile to the a priori information, while if the adopted σ_a^2 values (diagonal elements of $\mathbf{S}_\mathrm{a}$) are too large, solutions rely mostly on the spectral measurement but may have the tendency to oscillate.

Here we take a priori information for both species from the Aura MLS data sets, considered to be accurately validated estimates for the quantities under investigation. All of the MLS O_3 and HNO_3 profiles measured over the GBMS observing periods (approximately from mid-January to mid-March 2010, 2011, and 2012 for HNO_3, 2011 and 2012 for O_3) within 1° latitude and 8° longitude from Thule are averaged together to give one O_3 and one HNO_3 profile. Using a single a priori for each of the two data sets ensures that the interannual differences as well as the seasonal evolution observed in the GBMS data sets do not depend on the a priori. Although the choice of MLS averages as a priori information for the GBMS deconvolution process might appear questionable, it should be noted that the differences between GBMS and MLS profiles are entirely independent of the specific a priori profile employed (Connor et al., 2007, Eq. 3). Moreover, in the altitude range of interest, both O_3 and HNO_3 GBMS retrievals are strongly dependent on the measured spectra and largely independent of the a priori (see Sects. 3.1 and 3.2).

For O_3 retrievals we choose a priori profile variances (diagonal elements of $\mathbf{S}_\mathrm{a}$) varying from 50 to 80 % depending on altitude and consider a correlation length of 5 km between gas concentrations at different altitudes. $\mathbf{S}_\mathrm{a}$ is held constant for the analysis of the entire data set. We assume the covariance matrix of the measurement vectors

AMTD
6, 2979–3011, 2013

to be diagonal, with all the diagonal elements σ_ε^2 equal, and use these diagonal elements as adjustable parameters for optimizing the retrieval sensitivity. In particular, we choose the smallest value (corresponding to the highest resolution) producing solution profiles which do not display unphysical oscillations. The σ_ε^2 eventually adopted is also held constant throughout the analysis and is of the same order of magnitude as the O_3 spectral residuals (i.e., the differences between the measured spectra and those generated from the retrieved profiles using the forward model).

Since HNO_3 spectra are characterized by many HNO_3 lines blended by pressure broadening and contaminated by a weak ozone line and by the tail of an intense O_3 emission outside the pass band, they are more problematic for retrievals, and are thus inverted using a two-step process. At the first step, the HNO_3 and O_3 signatures appearing in the GBMS pass band are simultaneously retrieved with $\mathbf{S}_a$ and $\mathbf{S}_\varepsilon$ matrices chosen following the same criteria adopted for the O_3 retrieval. In order to extract more information from the HNO_3 emission, the O_3 background obtained at the first step is subtracted from the overall observed spectral signal and the resulting HNO_3 only spectrum is then inverted again with a larger weight placed on the spectral measurement (smaller σ_ε^2 values) with respect to the a priori profile. This second phase, aimed at maximizing the sensitivity and vertical resolution of the HNO_3 retrieval, cannot be achieved in the presence of the O_3 background signal. The HNO_3 only spectrum is inverted using the same a priori profile and $\mathbf{S}_a$ matrix employed in the first inversion, but with σ_ε values which are different from spectrum to spectrum and are assigned to be proportional to the spectral noise (estimated using the RMS of the spectral residual measured at the first step of the inversion process).

Spectroscopic parameters necessary to calculate the absorption coefficients for a given molecular transition are taken from the Jet Propulsion Laboratory (JPL) spectral catalog (available at http://spec.jpl.nasa.gov) (Pickett et al., 1998) (lines intensities) and from the HITRAN2008 database (Rothman et al., 2009) (pressure broadening and temperature dependence coefficients). Atmospheric pressure and temperature profiles

AMTD
6, 2979–3011, 2013

used for the analysis in this study are obtained from MLS observations for the specific dates and location.

3.1 O_3 retrievals

In Fig. 1 the retrieval results for the GBMS O_3 spectrum recorded at Thule on 20 February 2011 are presented. Panel a shows the spectrum observed by GBMS and, superimposed, the spectrum calculated from the corresponding OE retrieved profile (displayed in panel c together with the a priori profile); the difference between the two spectra (spectral residual) is drawn in panel b. Panel e depicts the Averaging Kernel functions (AVKs), which are the rows of the Averaging Kernel matrix, defined in the OE method as $\mathbf{A} = \partial \boldsymbol{x}_r / \partial \boldsymbol{x}$ (e.g., Rodgers, 2000). Each AVK represents the sensitivity of the retrieval at a given altitude to variations in the true atmospheric state at all altitudes. When they are well-peaked functions, centered at their nominal altitude, a perturbation in the true atmospheric state is attributed to the correct altitude in the retrieved profile. Furthermore, the area enclosed under each kernel is an indication of the total sensitivity of the retrieved profile at that altitude to atmospheric variations. Sensitivity values close to 1 indicate that the major contribution to the solution comes from the spectral measurement rather than from the a priori. In the altitude range where both these conditions (correspondence between the AVKs' nominal and peak altitude; sensitivity close to 1) are satisfied, the retrieval responds satisfactorily to changes in the atmospheric state, and the AVKs' full width at half maximum (FWHM) can be used as a rough measure of the local vertical resolution of the obtained mixing ratio vertical profile.

Results shown in panels e, f and g suggest that our retrieval has good sensitivity ($> 80\,\%$) in the vertical range $\sim$17–50 km, where the difference between the nominal and the peak height of the AVKs does not exceed 3 km and the vertical resolution is between $\sim$9 and 18 km (but remains under 12 km up to 44 km). This is the vertical range over which GBMS O_3 profiles may be used for scientific purposes. Finally, panel d shows the total error on the retrieved profile with its different contributions. Errors on GBMS profiles are mainly due to instrument calibration and data scaling procedures

AMTD
6, 2979–3011, 2013

(∼ 8 %) (Parrish et al., 1988; Cheng et al., 1996), and to parameters used in the forward model calculation (7 %). These two contributions add up (in quadrature) to an overall $\pm 1\,\sigma$ of ∼ 11 % (red dashed line). The uncertainties related to the calibration and data scaling (e.g., errors in receiver temperature and atmospheric opacity) can be both systematic and random, also depending on the time periods considered and local weather conditions (most likely systematic during short periods of very stable weather and random over long periods comprising different field campaigns). Similarly, we consider spectroscopic parameters as a source of systematic error, whereas pressure and temperature vertical profiles cause mostly random errors. As a distinction between fixed and variable errors is not always possible in this context, we conservatively consider all the above mentioned uncertainties to be systematic. The error due to measurement noise (green dashed dotted line), determined following the OE procedure presented in Connor (1995), gives a small contribution (< 0.05 ppm at all altitudes) to the overall uncertainty.

One additional error source (not included in the plot of Fig. 1d) is the limited vertical resolution of the observing technique. This lack of resolution leads to solution profiles that are a smoothed version of the true atmospheric state and that do not exhibit the fine vertical structure of the original profiles. Many authors in the OE literature suggest that this error, called "smoothing error", should be estimated only if accurate knowledge of the variability of the fine structure of the true atmosphere is available (Connor, 1995; Rodgers, 2000). We follow this prescription and do not include the smoothing error in our error estimate. Additionally, this resolution error can be completely removed from comparisons with data sets with a higher vertical resolution (e.g., the Aura MLS data in this work) by "convolving" the higher resolution profiles with the AVKs of the lower resolution data (GBMS):

$$\boldsymbol{x}_{\mathrm{conv}} = \boldsymbol{x}_{\mathrm{a}} + \mathbf{A}_{\mathrm{GBMS}} \left(\boldsymbol{x}_{\mathrm{MLS}} - \boldsymbol{x}_{\mathrm{a}} \right) \tag{2}$$

The total uncertainty of the retrieved profiles, determined by adding in quadrature the above mentioned contributions, generally amounts to 11 % (blue line), with a minimum

AMTD
6, 2979–3011, 2013

absolute error of 0.2 ppmv and small differences depending on observing conditions. The reader is directed to Fiorucci et al. (2011) for more details on the error analysis.

3.2 HNO_3 retrievals

An illustrative inversion of the HNO_3 spectrum (after the subtraction of the O_3 background line) is presented in Fig. 2. Similarly to Fig. 1, the measured and forward-model generated spectra are presented in panel a, their difference in panel b, the a priori and retrieved mixing ratio profiles in panel c and the uncertainties on the retrieved profiles in panel d. Panels e and f depict the AVKs with their sensitivity curve, and the FWHM of the kernels, respectively. Differences between the nominal height of each AVK and the actual height where it peaks are shown in panel g. Figure 2 (panels e and g) shows that the AVKs are well peaked and centered close to their correct altitude level in the vertical range 17–45 km, with their sensitivity close to 1. The vertical resolution varies from 9 to 14 km in this vertical range (panel f), which is the one recommended for scientific use of the GBMS HNO_3 data set.

The total uncertainty has been assessed following the same criteria used for O_3 and is given by the larger of 15 % or 0.2 ppbv (see also Fiorucci et al., 2011), with the main contribution given by uncertainties due to calibration and to parameters used in the forward model calculation.

4 Correlative data sets

The Microwave Limb Sounder (MLS) is one of four instruments aboard Aura, the latest NASA Earth Observing System satellite, launched on 15 July 2004 into a near-polar, sun-synchronous orbit (Waters et al., 2006; Schoeberl et al., 2006). Aura MLS observes several atmospheric constituents by measuring millimeter and submillimeter wavelength thermal emission from Earth's limb using five broad spectral bands between 118 GHz and 2.5 THz. The Aura orbit and MLS viewing geometry (viewing

AMTD
6, 2979–3011, 2013

forward along the flight direction and vertically scanning the limb) lead to data coverage from 82° S to 82° N latitude on every orbit, with ∼13 orbits per day (Santee et al., 2007).

MLS mixing ratio vertical profiles are retrieved using an algorithm based on the Optimal Estimation method (Livesey et al., 2006). All the data presented in this comparison are processed with the version 3.3 (v3.3) algorithms, the third "public release" of MLS data. Main changes, improvements, and issues with v3.3 data are discussed in the v3.3 MLS data quality document (Livesey et al., 2011; http://mls.jpl.nasa.gov/data/datadocs.php).

4.1 Aura MLS O_3 observations

The MLS O_3 standard product for version 3.3 is taken from the 240 GHz retrieval and is recommended for scientific use over the range 261 to 0.02 hPa. Based on the FWHM of the Averaging Kernels, the vertical resolution is ∼2.5 km in the uppermost troposphere and stratosphere, whereas the horizontal (along-track) resolution varies from 300 to 450 km. The cross-track resolution, determined by the 240 GHz radiometer field of view, is fixed at 6 km. The single-profile precision ranges between 0.02 and 0.2 ppmv in the same vertical range (i.e., uppermost troposphere and stratosphere). Ozone profiles from v3.3 are very similar to v2.2 profiles in the stratosphere and above, so the stratospheric results reported in v2.2 validation papers (Froidevaux et al., 2008; Jiang et al., 2007; Livesey et al., 2008) generally hold for the v3.3 product as well. All these studies show generally good agreement (within 5–10 %) between MLS data and satellite, balloon, aircraft, and ground-based measurements. More detailed information on the useful vertical range, resolution and precision of the v3.3 O_3 data, as well as results from comparisons with other data sets, can be found in Sect. 3.17 of Livesey et al. (2011).

AMTD
6, 2979–3011, 2013

4.2 Aura MLS HNO_3 observations

The HNO_3 product is derived from the 240 GHz radiometer for atmospheric pressures equal to or greater than 22 hPa and from the 190 GHz radiometer at higher altitudes. MLS HNO_3 retrievals have been greatly improved in v3.3. Comparisons with correlative satellite and ground-based data sets suggest that the low bias (∼ 10–30 %) observed throughout most of the stratosphere in the v2.2 HNO_3 profiles has been largely removed in v3.3. The latter profiles are recommended for scientific use over the range 215–1.5 hPa, with a single-profile precision, empirically estimated, of ∼ 0.6–0.7 ppbv throughout the range from 100 to 3.2 hPa, below and above which it increases sharply. The effects of systematic uncertainties on v3.3 measurements have not been completely assessed but are expected to be very similar to those estimated for v2.2 (measurement biases varying with altitude between ±0.5 and ±2 ppbv and multiplicative errors of ±5–15 % throughout the stratosphere). The vertical resolution varies between 3 and 5 km, depending on altitude. The along-track horizontal resolution is 450–500 km over most of the vertical range, whereas the cross-track resolution, set by the width of the field of view of the 190 GHz and 240 GHz radiometers, is ∼ 10 km.

5 Comparison criteria

Being in near-polar orbit, Aura MLS provides each day closely spaced observations near high latitude sites. Thus, a choice of MLS overpasses close to Thule is available daily for the intercomparison of GBMS and MLS profiles. However, particularly non-homogeneous conditions characteristic of polar winter/spring periods are likely to compromise the comparison results, and stringent coincidence criteria (both spatial and temporal) are required. Dynamical, chemical and microphysical processes, including rapid ClO activation (and consequent O_3 depletion) and HNO_3 sequestration in PSCs, can induce strong spatial and temporal concentration gradients in both considered species. In order to overcome these issues, for each GBMS measurement we first

AMTD
6, 2979–3011, 2013

select MLS observations within a box of ±1° latitude and ±8° longitude from the GBMS observing site. Then, among the selected MLS profiles, we choose the closest in time to the GBMS measurement, discarding those that are more than 6 hours away from the limits of the GBMS integration interval. Using the above mentioned requirements, we obtain a total of 43 coincidences between GBMS and MLS for the HNO_3 comparison (7 in 2010, 19 in 2011 and 17 in 2012) and 54 for the O_3 (27 both in 2011 and 2012). Sensitivity tests have been carried out to make sure that the comparison results do not change significantly if more stringent spatial and temporal selection criteria are employed. We first examine the sensitivity of the results to the box size, testing a reduced box of ±0.5° latitude and ±4° longitude. Then the time criterion is investigated, selecting MLS data within ±3 h from GBMS observations. These tests show that the stricter constraints on both spatial and temporal matching criteria reduce the number of coincidences without significantly modifying the comparison results.

Two additional criteria are used to select air masses which have experienced similar dynamical and chemical conditions: the Potential Vorticity (PV), useful to differentiate inner vortex from extra vortex air, and the temperature, which is a key parameter in chemical processes within the polar vortex. In order to include these criteria in our selection procedure, we have examined daily maps with analysis of PV and temperature values at 550 K provided by the Danish Meteorological Institute. PV values between 70 and 80×10^{-6} K m^2 s^{-1} kg^{-1} are used to identify the vortex edge, while 192 K is considered the formation temperature threshold for type I PSCs at this altitude (assuming a 10 ppbv concentration of HNO_3 and 5 ppmv of H_2O) (Larsen et al., 1997, 2000).

By using these proxies we eliminate from the comparison those profile pairs in which GBMS and MLS sampled air masses on opposite sides of the vortex edge or matches when either or both instruments looked inside the area of possible formation of PSCs. The latter selection process does not affect the results, and therefore in order to increase the statistical significance of the intercomparison we did not implement it in the end. Finally, MLS data that did not pass all the v3.3 quality control criteria and GBMS measurements for which the observed spectrum has been poorly fitted by the retrieval

AMTD
6, 2979–3011, 2013

algorithm have been left out of the comparison. Because of the different vertical resolutions of the instruments (see Sects. 3.1, 3.2, 4.1 and 4.2), before the selected pairs of measurements are compared, the higher resolution MLS profiles are interpolated to the GBMS retrieval grid and smoothed using the appropriate GBMS AVKs and a priori profile.

6 Results

In Figs. 3, 4 and 5 (6, 7 and 8) we present results of comparisons of stratospheric O_3 (HNO_3) from Aura MLS v3.3 and GBMS. Figure 3a shows MLS and GBMS O_3 mean profiles obtained by averaging together 54 observations from the years 2011 and 2012. Panels b and c of Fig. 3 illustrate absolute and percent differences, respectively, between the convolved MLS and GBMS O_3 profiles, with dashed lines indicating $\pm 1\,\sigma$ of the mean difference. The two data sets display good agreement up to 26 km, with the GBMS being lower than the convolved MLS by less than 0.5 ppmv. Above 26 km the agreement worsens with increasing altitude, with a maximum difference of ~ 0.9 ppmv ($\sim 18\,\%$) near the profile peak, after which the GBMS-MLS absolute difference decreases again.

In order to investigate the correlation between MLS and GBMS O_3 data presented in Fig. 3, Fig. 4 shows time series of all the selected MLS-GBMS pairs of values at three altitude levels (22, 32 and 40 km). As mentioned in Sect. 5, to account for the different vertical resolution between the ground- and the satellite-based data, each MLS profile has been convolved with the respective GBMS set of AVKs before the comparison. For the purpose of illustrating the effect of the convolution on MLS O_3 profiles, in Fig. 4 we show both the original (red stars) and the convolved (red open circles) values. The red and blue shaded areas represent the uncertainties on MLS (convolved) and GBMS O_3 data, respectively. The indicated MLS uncertainty includes both systematic and random errors, whereas the GBMS error bars are calculated as described in Sect. 3.1.

AMTD
6, 2979–3011, 2013

Figure 4 shows that GBMS O_3 mixing ratio values track MLS daily variations reasonably well, and confirms that the former data set has a low bias with respect to the satellite observations, with a difference that is essentially consistent in both years and depends on the altitude level. In order to evaluate the capability of GBMS measurements to follow seasonal and interannual O_3 variations (e.g., to quantify the springtime ozone loss), a scatterplot of MLS vs GBMS O_3 partial column contents integrated between 17 and 50 km (the altitude range over which GBMS profiles are considered reliable) is displayed in Fig. 5a. A correlation coefficient of 0.73 and a slope of 0.78 for the linear fit to the data indicate a generally good correlation between the two data sets, with the GBMS O_3 values having a larger variability with respect to MLS data. If the same plot is drawn for column contents between 20 and 50 km (Fig. 5b), thus excluding the bottom 3 km of the altitude range considered scientifically meaningful, then the correlation improves to a coefficient of 0.86 and a slope of 0.97. This suggests that the O_3 partial column variations detected by the GBMS agree well with those measured by the Aura MLS, particularly from 20 km upwards.

Figures 6, 7 and 8 are analogous to Figs. 3, 4 and 5, but concern HNO_3 measurements. MLS and GBMS HNO_3 peak absolute values (Fig. 6) agree fairly well. Figure 6b shows a positive bias of GBMS versus MLS measurements, reaching a maximum of ~ 1 ppbv (10 %) near the profile peak. This bias decreases above the profile peak and becomes negative above 26 km. The agreement between the two data sets remains within $\pm 1\,\sigma$ of the mean absolute difference over the whole vertical range (Fig. 6b).

Figure 7 shows that GBMS HNO_3 measurements are generally well correlated with both the original and the convolved MLS observations during the three years at all altitudes. However, at 18 km the agreement between the original and the convolved satellite data is worse than it is at higher levels because the lower vertical resolution of the ground-based observations does not allow the particular fine structure of the original HNO_3 profiles to be captured. In Fig. 8 the correlation coefficient (0.92) and the slope of the linear fit (0.95) indicate that the partial columns of the two data sets (integrated over the GBMS vertical range suggested for scientific use) are well correlated

AMTD
6, 2979–3011, 2013

and therefore their variations are in close agreement. In contrast to the O_3 case, for HNO_3 the correlation parameters do not change significantly when the altitude interval over which the column contents are calculated is changed. This discrepancy between the two sets of comparisons is under investigation.

GBMS HNO_3 observations from mid-latitudes have been previously compared to Aura MLS measurements. In particular, GBMS measurements carried out at the Alpine site of Testa Grigia (45.9° N, 7.7° E, elev. 3500 m) in 2005 were found to be ∼3 ppbv (20–30 %) higher than satellite data near the profile peak (Santee et al., 2007). However, both the GBMS and the MLS retrieval algorithms have been revised since then. Fiorucci et al. (2011) compared GBMS profiles retrieved applying the "old" and the "new" techniques to the same set of spectra, finding that the former set of profiles (v1) were systematically larger near the peak by up to 2 ppbv with respect to v2 profiles. On the other hand, as seen in Sect. 4.2, MLS HNO_3 values have increased from v2.2 to v3.3 by about 20–30 % throughout most of the stratosphere (Livesey et al., 2011). A GBMS versus MLS HNO_3 intercomparison plot obtained using the most recent algorithms applied to mid-latitude observations during winters 2004/2005, 2005/2006, and 2006/2007 is shown in Livesey et al. (2011) (on p. 88). The above-mentioned results suggest that, on average, GBMS and MLS HNO_3 data from the mid-latitudes compare to one another similarly to what is shown in this work for the high latitudes, with the GBMS displaying a small but non-negligible high bias at the HNO_3 mixing ratio peak.

7 Summary and conclusions

In this study we present O_3 and HNO_3 GBMS measurements obtained at the NDACC station in Thule, Greenland, during the last two (for O_3) or three (for HNO_3) winters. We give a characterization of the retrieved profiles (altitude range of sensitivity, vertical resolution, total uncertainty) and assess their accuracy by comparing them with the well-validated Aura MLS observations. This is relevant to the scientific community since the GBMS O_3 and HNO_3 retrievals are publicly available on the NDACC database and

AMTD
6, 2979–3011, 2013

may be used in future studies on the Arctic winter stratosphere. Moreover, in the event that operational satellite missions would be reduced in the future, it is useful to assess to what extent ground-based microwave instruments can help to fill the consequent gaps in atmospheric data.

In this work it is shown that GBMS O_3 profiles can be considered for scientific use between ∼17 and ∼50 km, with an overall 1 σ uncertainty that amounts to the larger of ∼11 % or 0.2 ppmv and a vertical resolution between about 9 and 18 km. Similarly, HNO_3 measurements have good sensitivity over the range ∼17–45 km and a vertical resolution encompassed between about 9 and 14 km in this altitude range. The 1 σ uncertainty is given by the larger of 15 % or 0.2 ppbv.

Results presented in section 6 illustrate that the GBMS O_3 mean profile displays a negative bias with respect to MLS throughout the considered altitude range. However, the difference between the two averaged profiles remains below 0.5 ppmv (∼10 %) in the lower stratosphere and below 0.9 (∼18 %) ppmv in the mid- to upper stratosphere. Morevoer, GBMS and MLS O_3 mixing ratio values correlate reasonably well at all altitudes, with very good results found for partial columns calculated from 20 km upwards.

The averaged GBMS HNO_3 profile shows values that are larger than those measured by MLS, with differences below ∼10 % (1 ppbv at the mixing ratio peak), up to 26 km. Upwards the absolute difference decreases and becomes negative. Timeseries of GBMS and MLS HNO_3 values at three different altitude levels and partial column variations (from 17 km upwards) show that the ground-based and the satellite HNO_3 data are well correlated.

Furthermore, the overall agreement between Aura MLS and GBMS HNO_3 observations has significantly improved since their previous intercomparison at mid-latitudes (Santee et al., 2007). This is consistent with changes made in the meantime in both the GBMS and the MLS retrieval algorithms.

We showed that GBMS retrievals may be successfully used to follow seasonal and interannual O_3 and HNO_3 variations in the Arctic winter stratosphere, as long as the estimated uncertainty and vertical resolution are taken into account. In fact, the poor

AMTD
6, 2979–3011, 2013

vertical resolution of the GBMS HNO_3 profiles affects the GBMS capability of depicting correctly the removal of gas-phase HNO_3, when the latter occurs over limited altitude ranges, but these data does represent a valuable asset for estimating column gas-phase HNO_3 removal upwards of 17 km. Similarly, GBMS O_3 measurements are proven capable of providing a useful quantitative estimate of the springtime ozone loss.

Acknowledgements. This material is based on work also supported by the National Science Foundation under grant 0936365 and by the Programma Nazionale di Ricerca in Antartide (PNRA) under grant 2009/A3.04. G. Muscari is indebted to Bob de Zafra for designing, building, and upgrading the GBMS, as well as for the economic and technical support that led to many successful GBMS field campaigns. We thank Pietro Paolo Bertagnolio, Svend Erik Ascanius, Claudia Di Biagio, and Giorgio di Sarra for their technical assistance during the GBMS field campaigns at Thule. Work at the Jet Propulsion Laboratory, California Institute of Technology, was done under contract with NASA.

References

Boyd, I. S., Parrish, A. D., Froidevaux, L., von Clarmann, T., Kyrölä, E., Russell III, J. M., and Zawodny, J. M.: Ground-based microwave ozone radiometer measurements compared with Aura-MLS v2.2 and other instruments at two Network for Detection of Atmospheric Composition Change sites, J. Geophys. Res., 112, D24S33, doi:10.1029/2007JD008720, 2007.

Cheng, D., de Zafra, R. L., and Trimble, C.: Millimeter wave spectroscopic measurements over the South Pole, 2. An 11-month cycle of stratospheric ozone observations during 1993–1994, J. Geophys. Res., 101, 6781–6793, 1996.

Connor, B. J., Barrett, J. W., Parrish, A., Solomon, P. M., De Zafra, R. L., and Jaramillo, M.: Ozone Over McMurdo Station, Antarctica, Austral Spring 1986: Altitude Profiles for the Middle and Upper Stratosphere, J. Geophys. Res., 92, 13221–13230, doi:10.1029/JD092iD11p13221, 1987.

Connor, B. J., Parrish, A., Tsou, J. J., and McCormick, M. P.: Error analysis for the ground-based microwave ozone measurements during STOIC, J. Geophys. Res., 100, 9283–9291, doi:10.1029/94JD00413, 1995.

Connor, B. J., Mooney, T., Barrett, J., Solomon, P., Parrish, A., and Santee M.: Comparison of ClO measurements from the Aura Microwave Limb Sounder to ground-based microwave

AMTD
6, 2979–3011, 2013

measurements at Scott Base, Antarctica, in spring 2005, J. Geophys. Res., 112, D24S42, doi:10.1029/2007JD008792, 2007.

de Zafra, R. L.: The ground-based measurements of stratospheric trace gases using quantitative millimeter wave emission spectroscopy, in Diagnostic tools in atmospheric physics, Proceedings of the international school of physics "Enrico Fermi", 23–54, Società italiana di fisica, Bologna, 1995.

de Zafra, R. L., Jaramillo, M., Parrish, A., Solomon, P. M., Connor, B., and Barrett, J.: High concentrations of chlorine monoxide at low altitudes in the Antarctic spring stratosphere: Diurnal variation, Nature, 328, 408–411, 1987.

de Zafra, R. L., Chan, V., Crewell, S., Trimble, C., and Reeves, J. M.: Millimeter wave spectroscopic measurements over the South Pole: 3. The behavior of stratospheric nitric acid through polar fall, winter, and spring, J. Geophys. Res., 102, 1399–1410, 1997.

Di Biagio, C., Muscari, G., di Sarra, A., de Zafra, R. L., Eriksen, P., Fiorucci, I., and Fuà, D.: Evolution of temperature, O_3, CO, and N_2O profiles during the exceptional 2009 Arctic major stratospheric warming as observed by lidar and mm-wave spectroscopy at Thule (76.5° N, 68.8° W), Greenland, J. Geophys. Res., 115, D24315, doi:10.1029/2010JD014070, 2010.

Fiorucci, I., Muscari, G., Bianchi, C., Di Girolamo, P., Esposito, F., Grieco, G., Summa, D., Bianchini, G., Palchetti, L., Cacciani, M., Di Iorio, T., Pavese, G., Cimini, D., and de Zafra, R. L.: Measurements of low amounts of precipitable water vapor by millimeter wave spectroscopy: An intercomparison with radiosonde, Raman lidar, and Fourier transform infrared data, J. Geophys. Res., 113, D14314, doi:10.1029/2008JD009831, 2008.

Fiorucci, I., Muscari, G., and de Zafra, R. L.: Revising the retrieval technique of a long-term stratospheric HNO_3 data set: from a constrained matrix inversion to the optimal estimation algorithm, Ann. Geophys., 29, 1317–1330, doi:10.5194/angeo-29-1317-2011, 2011.

Froidevaux, L., Jiang, Y. B., Lambert, A., Livesey, N. J., Read, W. G., Waters, J. W., Browell, E. V., Hair, J. W., Avery, M. A., McGee, T. J., Twigg, L. W., Sumnicht, G. K., Jucks, K. W., Margitan, J. J., Sen, B., Stachnik, R. A., Toon, G. C., Bernath, P. F., Boone, C. D., Walker, K. A., Filipiak, M. J., Harwood, R. S., Fuller, R. A., Manney, G. L., Schwartz, M. J., Daffer, W. H., Drouin, B. J., Cofield, R. E., Cuddy, D. T., Jarnot, R. F., Knosp, B. W., Perun, V. S., Snyder, W. V., Stek, P. C., Thurstans, R. P., and Wagner, P. A.: Validation of Aura Microwave Limb Sounder stratospheric ozone measurements, J. Geophys. Res., 113, D15S20, doi:10.1029/2007JD008771, 2008.

AMTD
6, 2979–3011, 2013

Haefele, A., De Wachter, E., Hocke, K., Kampfer, N., Nedoluha, G. E., Gomez, R. M., Eriksson, P., Forkman, P., Lambert, A., and Schwartz, M. J.: Validation of ground-based microwave radiometers at 22 GHz for stratospheric and mesospheric water vapor, J. Geophys. Res., 114, D23305, doi:10.1029/2009JD011997, 2009.

Harris, N. R. P., Lehmann, R., Rex, M., and von der Gathen, P.: A closer look at Arctic ozone loss and polar stratospheric clouds, Atmos. Chem. Phys., 10, 8499–8510, doi:10.5194/acp-10-8499-2010, 2010.

Hoffmann, C. G., Raffalski, U., Palm, M., Funke, B., Golchert, S. H. W., Hochschild, G., and Notholt, J.: Observation of strato-mesospheric CO above Kiruna with ground-based microwave radiometry –retrieval and satellite comparison, Atmos. Meas. Tech., 4, 2389–2408, doi:10.5194/amt-4-2389-2011, 2011.

Jiang, Y. B., Froidevaux, L., Lambert, A., Livesey, N. J., Read, W. G., Waters, J. W., Bojkov, B., Leblanc, T., McDermid, I. S., Godin-Beekmann, S., Filipiak, M. J., Harwood, R. S., Fuller, R. A., Daffer, W. H., Drouin, B. J., Cofield, R. E., Cuddy, D. T., Jarnot, R. F., Knosp, B. W., Perun, V. S., Schwartz, M. J., Snyder, W. V., Stek, P. C., Thurstans, R. P., Wagner, P. A., Allaart, M., Andersen, S. B., Bodeker, G., Calpini, B., Claude, H., Coetzee, G., Davies, J., De Backer, H., Dier, H., Fujiwara, M., Johnson, B., Kelder, H., Leme, N. P., Konig-Langlo, G., Kyro, E., Laneve, G., Fook, L. S., Merrill, J., Morris, G., Newchurch, M., Oltmans, S., Parrondos, M. C., Posny, F., Schmidlin, F., Skrivankova, P., Stubi, R., Tarasick, D., Thompson, A., Thouret, V., Viatte, P., Vomel, H., von der Gathen, P., Yela, M., and Zablocki, G.: Validation of the Aura Microwave Limb Sounder Ozone by Ozonesonde and Lidar Measurements, J. Geophys. Res. 112, D24S34, doi:10.1029/2007JD008776, 2007.

Kuntz, M., Kopp, G., Berg, H., Hochschilda, G., and Krupa, R.: Joint retrieval of atmospheric constituent profiles from ground-based millimetre-wave measurements: ClO, HNO_3, N_2O, and O_3, J. Geophys Res., 104, 13981–13992, 1997.

Larsen, N., Knudsen, B. M., Rosen, J. M., Kjome, N. T., Neuber, R., and Kyro, E.: Temperature histories in liquid and solid polar stratospheric cloud formation, J. Geophys. Res., 102, 23505–23517, 1997.

Larsen, N., Mikkelsen, I. S., Knudsen, B. M., Schreiner, J., Voigt, C., Mauersberger, K., Rosen, J. M., and Kjome, N. T.: Comparison of chemical and optical in situ measurements of polar stratospheric clouds, J. Geophys. Res., 105, 1491–1502, 2000.

Livesey, N. J., Snyder, W. V., Read, W. G., and Wagner, P. A.: Retrieval algorithms for the EOS Microwave Limb Sounder (MLS) instrument, IEEE T. Geosci. Remote, 44, 1144–1155, 2006.

AMTD
6, 2979–3011, 2013

Livesey, N. J., Filipiak, M. J., Froidevaux, L., Read, W. G., Lambert, A., Santee, M. L., Jiang, J. H., Pumphrey, H. C., Waters, J. W., Cofield, R. E., Cuddy, D. T., Daffer, W. H., Drouin, B. J., Fuller, R. A., Jarnot, R. F., Jiang, Y. B., Knosp, B. W., Li, Q. B., Perun, V. S., Schwartz, M. J., Snyder, W. V., Stek, P. C., Thurstans, R. P., Wagner, P. A., Avery, M., Browell, E. V., Cammas, J.-P., Christensen, L. E., Diskin, G. S., Gao, R.-S., Jost, H.-J., Loewenstein, M., Lopez, J. D., Nedelec, P., Osterman, G. B., Sachse, G. W., and Webster, C. R.: Validation of Aura Microwave Limb Sounder O_3 and CO observations in the upper troposphere and lower stratosphere, J. Geophys. Res., 113, D15S02, doi:10.1029/2007JD008805, 2008.

Livesey, N. J, Read, W. G., Froidevaux, L., Lambert, A., Manney, G. L., Pumphrey, H. C., Santee, M. L., Schwartz, M. J., Wang, S., Cofeld, R. E., Cuddy, D. T., Fuller, R. A., Jarnot, R. F., Jiang, J. H., Knosp, B. W., Stek, P. C., Wagner, P. A., and Wu, D. L.: Earth Observing System (EOS) Aura Microwave Limb Sounder (MLS) Version 3.3 Level 2 data quality and description document, available at: http://mls.jpl.nasa.gov/data/datadocs.php (last access: 20 February 2013), 2011.

Manney, G. L., Santee, M. L., Rex, M., Livesey, N. J., Pitts, M. C., Veefkind, P., Nash, E. R., Wohltmann, I., Lehmann, R., Froidevaux, L., Poole, L. R., Schoeberl, M. R., Haffner, D. P., Davies, J., Dorokhov, V., Gernandt, H., Johnson, B., Kivi, R., Kyro, E., Larsen, N., Levelt, P. F., Makshtas, A., McElroy, C. T., Nakajima, H., Parrondo, M. C., Tarasick, D. W., von der Gathen, P., Walker, K. A., and Zinoviev, N. S.: Unprecedented Arctic ozone loss in 2011, Nature, 478, 469–475, doi:10.1038/nature10556, 2011.

Muscari, G., Santee, M. L., and de Zafra, R. L.: Intercomparison of stratospheric HNO_3 measurements over Antarctica: Ground-Based Millimeter-wave versus UARS/MLS Version 5 retrievals, J. Geophys. Res., 107, 4809, doi:10.1029/2002JD002546, 2002.

Muscari, G., di Sarra, A. G., de Zafra, R. L., Lucci, F., Baordo, F., Angelini, F., and Fiocco, G.: Middle atmospheric O_3, CO, N_2O, HNO_3, and temperature profiles during the warm Arctic winter 2001–2002, J. Geophys. Res., 112, D14304, doi:10.1029/2006JD007849, 2007.

Muscari, G., Cesaroni, C., Fiorucci, I., Smith, A. K., Froidevaux, L., and Mlynczak M. G.: Stratomesospheric ozone measurements using ground-based millimeter-wave spectroscopy at Thule, Greenland, J. Geophys. Res., 117, D07307, doi:10.1029/2011JD016863, 2012.

Nedoluha, G. E., Gomez, R. M., Hicks, B. C., Helmboldt, J., Bevilacqua, R. M., and Lambert, A.: Ground-based microwave measurements of water vapor from the midstratosphere to the mesosphere, J. Geophys. Res., 116, D02309, doi:10.1029/2010JD014728, 2011.

AMTD
6, 2979–3011, 2013

Palm, M., Hoffmann, C. G., Golchert, S. H. W., and Notholt, J.: The ground-based MW radiometer OZORAM on Spitsbergen – description and status of stratospheric and mesospheric O_3-measurements, Atmos. Meas. Tech., 3, 1533–1545, doi:10.5194/amt-3-1533-2010, 2010.

Parrish, A., de Zafra, R. L., Solomon, P. M., and Barrett, J. W.: A ground-based technique for millimeter wave spectroscopic observations of stratospheric trace constituents, Radio Sci., 23, 106–118, 1988.

Parrish, A., Connor, B. J., Tsou, J. J., McDermid, I. S., and Chu, W. P.: Ground-Based Microwave Monitoring of Stratospheric Ozone, J. Geophys. Res., 97, 2541–2546, doi:10.1029/91JD02914, 1992.

Pickett, H. M., Poynter, R. L., Cohen, E. A., Delitsky, M. L., Pearson, J. C., and Müller, H. S. P.: Submillimeter, millimeter, and microwave spectral line catalog, J. Quant. Spectrosc. Ra., 60, 883–890, doi:10.1016/S0022-4073(98)00091-0, 1998.

Rex, M. Salawitch, R. J., Deckelmann, H., von der Gathen, P., Harris, N. R. P., Chipperfield, M. P., Naujokat, B., Reimer, E., Allaart, M., Andersen, S. B., Bevilacqua, R., Braathen, G. O., Claude, H., Davies, J., De Backer, H., Dier, H., Dorokhov, V., Fast, H., Gerding, M., Godin-Beekmann, S., Hoppel, K., Johnson, B., Kyrö, E., Litynska, Z., Moore, D., Nakane, H., Parrondo, M. C., Risley Jr., A. D., Skrivankova, P., Stübi, R., Viatte, P., Yushkov, V., and Zerefos, C.: Arctic winter 2005: Implications for stratospheric ozone loss and climate change, Geophys. Res. Lett., 33, L23808, doi:10.1029/2006GL026731, 2006.

Rodgers, C. D.: Retrieval of atmospheric temperature and composition from remote measurements of thermal radiation, Rev. Geophys. Space Ge., 14, 609–624, 1976.

Rodgers, C. D.: Inverse method for atmospheric sounding, Series on atmospheric, oceanic and Planetary Physics – Vol.2, Taylor, F. W., World Scientific Publishing Co. Pte LTd, Singapore, 2000.

Rothman, L. S., Gordon, I. E., Barbe, A., ChrisBenner, D., Bernath, P. F., Birk, M., Boudon, V., Brown, L. R., Campargue, A., Champion, J.-P., Chance, K., Coudert, L. H., Dana, V., Devi, V. M., Fally, S., Flaud, J.-M., Gamache, R. R., Goldman, A., Jacquemart, D., Kleiner, I., Lacome, N., Lafferty, W. J., Mandin, J.-Y., Massie, S. T., Mikhailenko, S. N., Miller, C. E., Moazzen-Ahmadi, N., Naumenko, O. V., Nikitin, A. V., Orphal, J., Perevalov, V. I., Perrin, A., Predoi-Cross, A., Rinsland, C. P., Rotger, M., Šimečkova, M., Smith, M. A. H., Sung, K., Tashkun, S. A., Tennyson, J., Toth, R. A., Vandaele, A. C., and VanderAuwera, J.: The HITRAN 2008 molecular spectroscopic database, J. Quant. Spectrosc. Ra., 110, 533–572, 2009.

AMTD
6, 2979–3011, 2013

Santee, M. L., Lambert, A., Read, W. G., Livesey, N. J., Cofield, R. E., Cuddy, D. T., Daffer, W. H., Drouin, B. J., Froidevaux, L., Fuller, R. A., Jarnot, R. F., Knosp, B. W., Manney, G. L., Perun, V. S., Snyder, W. V., Stek, P. C., Thurstans, R. P., Wagner, P. A., Waters, J. W., Muscari, G., deZafra, R. L., Dibb, J. E., Fahey, D. W., Popp, P. J., Marcy, T. P., Jucks, K. W., Toon, G. C., Stachnik, R. A., Bernath, P. F., Boone, C. D., Walker, K. A., Urban, J., and Murtagh, D.: Validation of Aura Microwave Limb Sounder HNO_3 Measurements, J. Geophys. Res., 112, D24S40, doi:10.1029/2007JD008721, 2007.

Schoeberl, M. R., Douglass, A. R., Hilsenrath, E., Bhartia, P. K., Barnett, J., Beer, R., Waters, J., Gunson, M., Froidevaux, L., Gille, J., Levelt, P. F., and DeCola, P.: Overview of the EOS Aura Mission, IEEE T. Geosci. Remote, 44, 1066–1074, 2006.

Solomon, S.: Progress towards a quantitative understanding of Antarctic ozone depletion, Nature, 347, 347–354, doi:10.1038/347347a0, 1990.

Twomey, S.: Introduction to the Mathematics of Inversion in Remote Sensing and Indirect Measurements, Developments in Geomathematics, Vol. 3, Elsevier Scientific Publ., Amsterdam, 1977.

Twomey, S., Herman, B., and Rabinoff R.: An extension of the Chahine method of inverting the radiative transfer equation, J. Atmos. Sci., 34, 1085–1090, 1977.

Waters, J. W., Froidevaux, L., Read, W. G., Manney, G. L., Elson, L. S., Flower, D. A., Jarnot, R. F., and Harwood, R. S.: Stratospheric ClO and ozone from the Microwave Limb Sounder on the Upper Atmosphere Research Satellite, Nature, 362, 597–602, 1993.

Waters, J. W., Froidevaux, L., Harwood, R. S., Jarnot, R. F., Pickett, H. M., Read, W. G., Siegel, P. H., Cofield, R. E., Filipiak, M. J., Flower, D. A., Holden, J. R., Lau, G. K., Livesey, N. J. Manney, G. L., Pumphrey, H. C., Santee, M. L., Wu, D. L., Cuddy, D. T. Lay, R. R., Loo, M. S., Perun, V. S., Schwartz, M. J., Stek, P. C., Thurstans, R. P., Boyles, M. A., Chandra, K. M., Chavez, M. C., Chen, G.-S., Chudasama, B. V., Dodge, R., Fuller, R. A., Girard, M. A., Jiang, J. H., Jiang, Y., Knosp, B. W., LaBelle, R. C., Lam, J. C., Lee, K. A., Miller, D., Oswald, J. E., Patel, N. C., Pukala, D. M., Quintero, O., Scaff, D. M., Snyder, W. V., Tope, M. C., Wagner, P. A., and Walch, M. J.: The Earth Observing System Microwave Limb Sounder (EOS MLS) on the Aura Satellite, IEEE T. Geosci. Remote, 44, 1075–1092, 2006.

World Meteorological Organization: Scientific Assessment of Ozone Depletion: 2010 Global Ozone Research and Monitoring Project, Report 52, 2011.

AMTD
6, 2979–3011, 2013

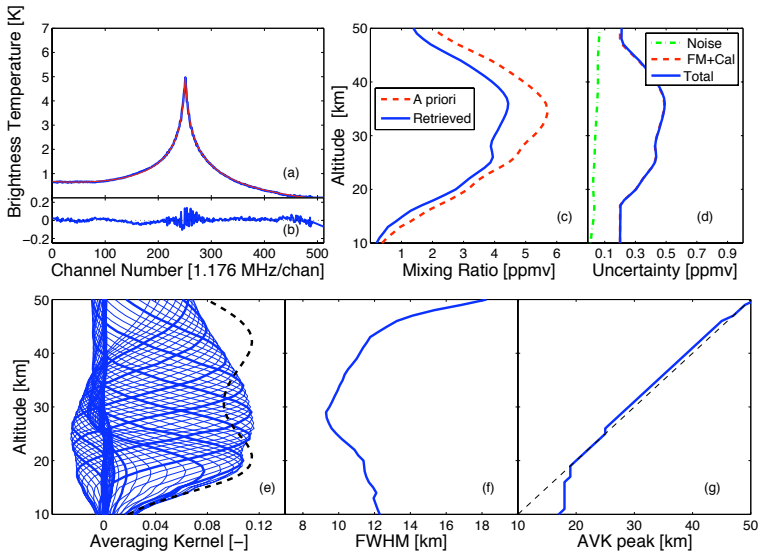

Fig. 1. Retrieval results for the GBMS O_3 spectrum recorded at Thule on 20 February 2011. **(a)** Spectrum observed by the GBMS (blue line) and forward model-generated from the OE retrieved profile (superimposed, in red). **(b)** Spectral residuals (measured spectrum minus forward-generated spectrum). **(c)** O_3 profile retrieved from the measured spectrum displayed in panel a (blue line) together with the a priori profile (red dashed line). **(d)** Total 1 σ uncertainty on the retrieved profile (in blue) with its different contributions: the red dashed line indicates uncertainty due to calibration, data scaling procedures and forward model parameters, the green dashed dotted line represents the uncertainty due to spectral noise. **(e)** GBMS Averaging Kernels (blue lines) and total sensitivity, as defined in the text, divided by 10 (dashed black line). Thicker blue lines are AVKs calculated at each 5 km altitude. **(f)** Vertical resolution of retrieved profile estimated as the FWHM of the AVKs. **(g)** Altitude of the peak of the AVKs versus their nominal altitude (blue line). The one-to-one line is also shown (dashed black).

AMTD
6, 2979–3011, 2013

Stratospheric O_3 and HNO_3 measurements over Thule

I. Fiorucci et al.

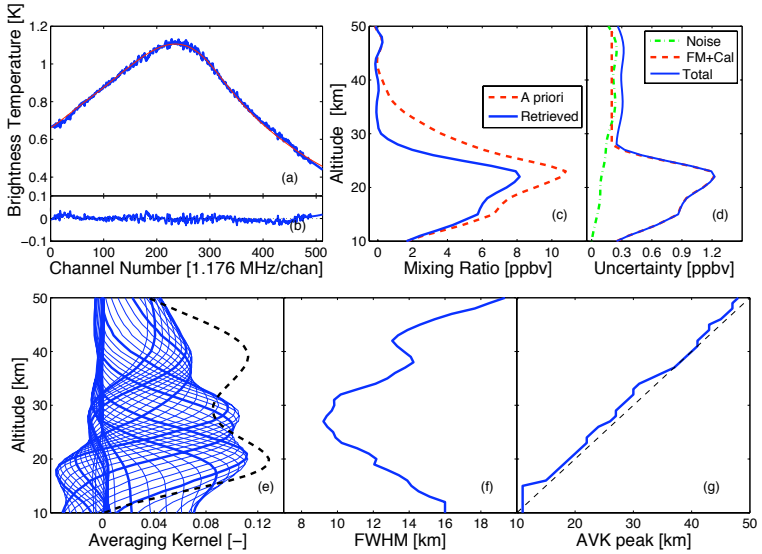

Fig. 2. As in Fig. 1, but for GBMS HNO_3 retrievals.

AMTD
6, 2979–3011, 2013

Stratospheric O_3 and HNO_3 measurements over Thule

I. Fiorucci et al.

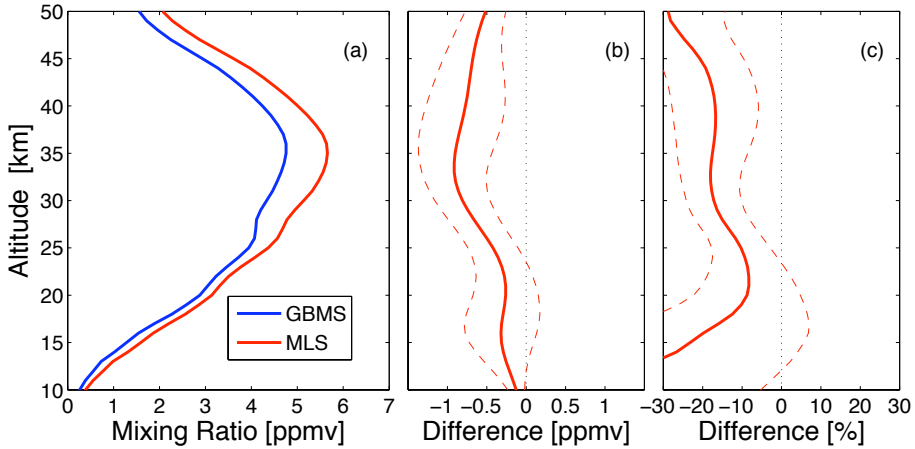

Fig. 3. Comparison of GBMS O_3 profiles with co-located Aura MLS observations obtained during the two winters 2011 and 2012 (54 coincidences). **(a)** GBMS (blue) and MLS convolved (red) mean profiles. **(b)** Mean absolute difference between GBMS and MLS convolved profiles. Dashed lines represent the standard deviation of the mean difference. **(c)** As in **(b)**, but indicating percent differences.

AMTD
6, 2979–3011, 2013

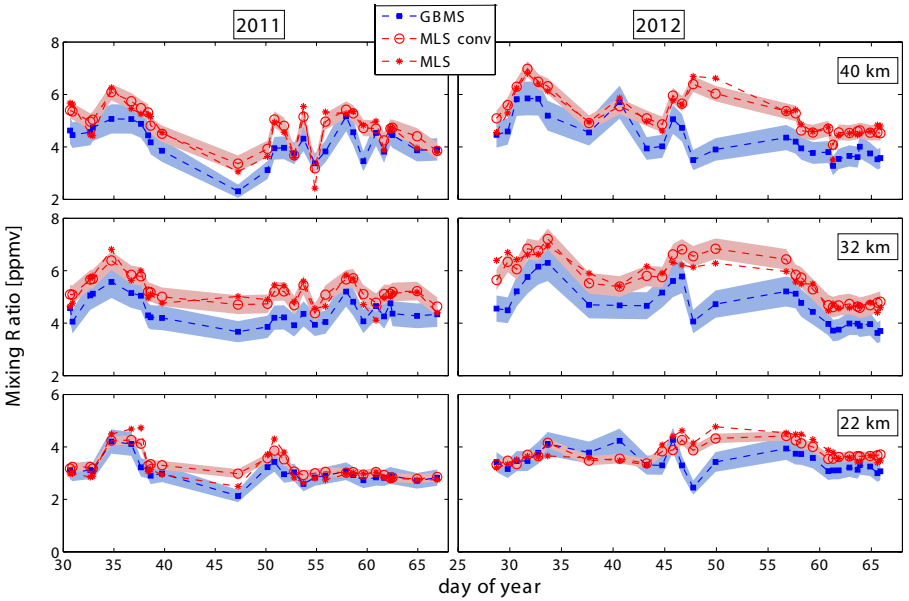

Fig. 4. Timeseries of GBMS (blue squares), Aura MLS (red stars) and convolved Aura MLS (open red circles) O_3 data for 2011 (left panels) and 2012 (right panels) at three altitude levels: 22 km, 32 km and 40 km. The blue shaded area depicts the GBMS uncertainty, calculated as described in Sect. 3.1 and shown in Fig. 1. Uncertainties on the convolved MLS data (red shaded area) include both systematic and random errors.

AMTD
6, 2979–3011, 2013

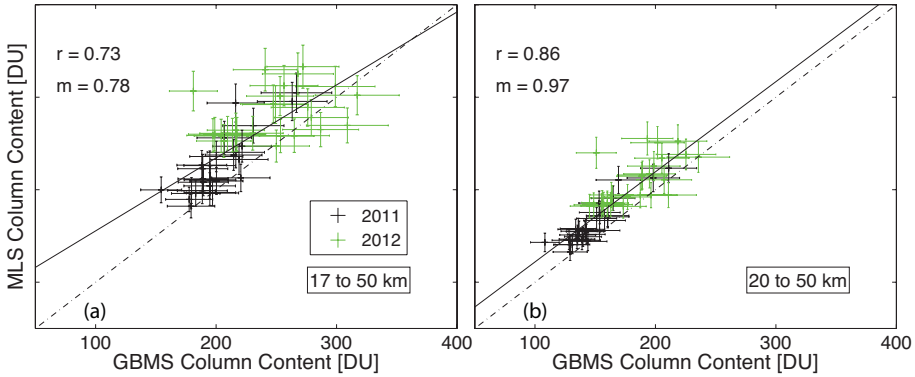

Fig. 5. (a) Scatterplot of Aura MLS against GBMS O_3 column content integrated between 17 and 50 km. Different colors denote different years: 2011 (black) and 2012 (green). Linear fit to the data points is displayed with a solid line, and the 1 : 1 bisector is represented with dash-dotted lines. The correlation coefficient (r) and the slope of the linear fit (m) are also reported. **(b)** As in **(a)**, but integrating between 20 and 50 km.

AMTD
6, 2979–3011, 2013

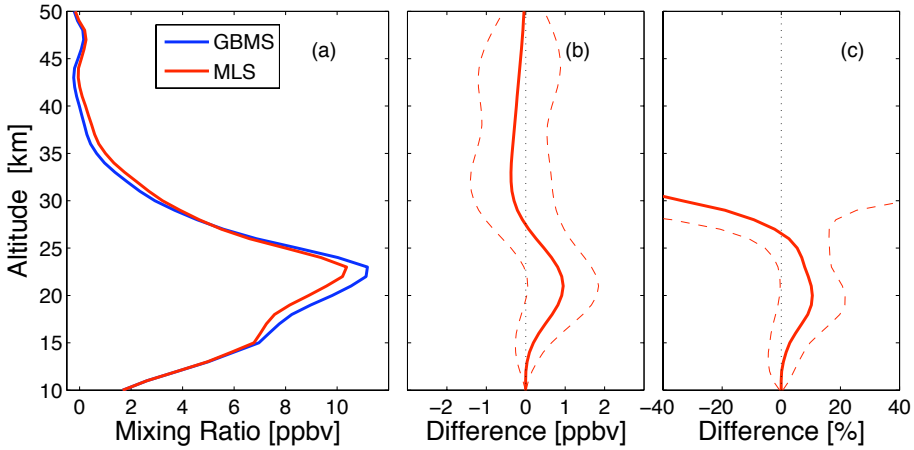

Fig. 6. Same as in Fig. 3, but for the HNO_3 intercomparison. A total of 43 coincidences was found.

AMTD
6, 2979–3011, 2013

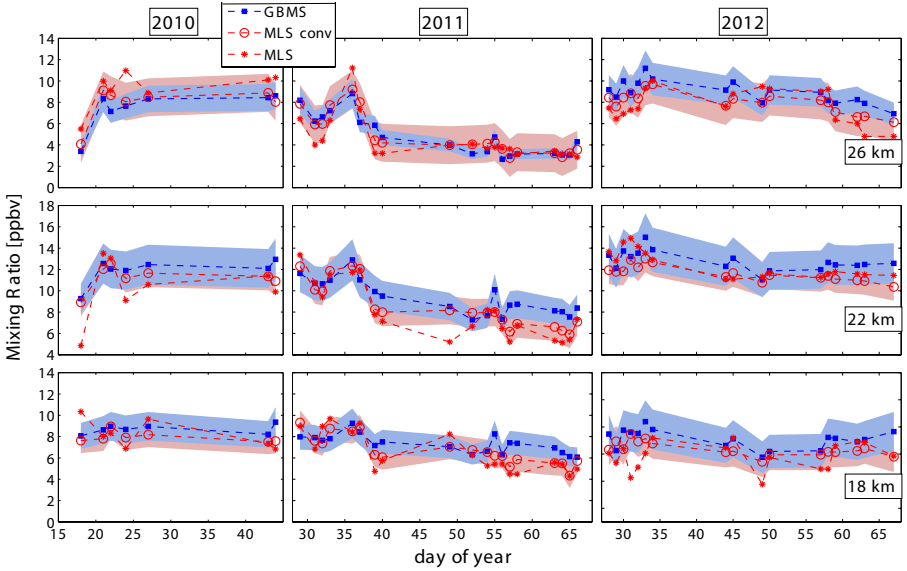

Fig. 7. Same as in Fig. 4, but for HNO_3 data. HNO_3 values are displayed at 18, 22 and 26 km altitude.

AMTD
6, 2979–3011, 2013

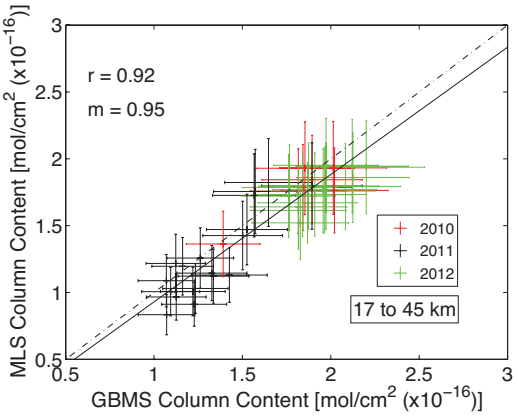

Fig. 8. Same as in Fig. 5, but for HNO_3 column content from 17 to 45 km altitude.

AMTD
6, 2979–3011, 2013